Precision Engineering 101 (2026) 256–273

Contents lists available at ScienceDirect

Precision Engineering

journal homepage: www.elsevier.com/locate/precision

Calibrating inter-target distances in a network with high accuracy using a terrestrial laser scanner

Bala Muralikrishnan [a,*], Meghan Shilling [a], Vincent Lee [a], Mary Gregg [b], Dennis Everett [a]

[a] Sensor Science Division, National Institute of Standards and Technology, Gaithersburg, MD, 20899, USA
[b] Statistical Engineering Division, National Institute of Standards and Technology, Boulder, CO, 80305, USA

ARTICLE INFO

Keywords:
Bundle-adjustment
Checkerboard/contrast targets
Network method
Performance evaluation
Self-calibration
Terrestrial laser scanner
Uncertainty

ABSTRACT

Self-calibration, as applied to terrestrial laser scanners (TLSs), is the process of estimating error model parameters from measurements made on a network of stationary targets from multiple TLS positions through a least-squares bundle adjustment. While the typical objective of self-calibration is to improve the accuracy of the TLS, we employ the technique to calibrate inter-target distances in the network with low uncertainty. We demonstrate the technique using two TLSs: a short-range, high-accuracy TLS and a long-range, low-accuracy TLS, in a 11 m × 6 m × 3 m space with 20 targets and four TLS positions. We obtain inter-target distance uncertainties of under 0.2 mm ($k = 2$) for the short-range TLS even when it was fully uncompensated (i.e., internal error model turned off) and under 0.35 mm ($k = 2$) for the long-range TLS. These uncertainties are substantially smaller, sometimes an order of magnitude smaller, than the errors typically expected from a TLS measurement of the same targets from a single position. We demonstrate the validity of our uncertainty estimates using a laser tracker as a reference. The calibrated network of targets can subsequently be used to evaluate the performance of the same TLS or other measurement instruments whose accuracy specifications are larger (typically, by at least a factor of four) than the uncertainties obtained by this method.

1. Introduction

Terrestrial laser scanners (TLSs) [1,2] are portable three-dimensional coordinate measuring instruments commonly used in geodesy and surveying, reverse engineering, manufacturing and assembly, crime scene investigation and reconstruction, historical monument digitization, etc. Periodic performance evaluation is critical to ensuring the instruments meet specifications, so the user has confidence in the data acquired. There are published documentary standards available, such as ASTM E3125-17 [3], ASTM E2538-15 [4], and ISO 17123-9 [5], that prescribe performance evaluation tests for TLSs.

Note that ASTM E2538-15 only prescribes a ranging test; this test has since been incorporated into the more comprehensive ASTM E3125-17. The tests described in the main body of ASTM E3125-17 require extensive equipment, a controlled environment, and are intended for instrument comparation and to make purchasing decisions. On the other hand, the tests described in ISO 17123-9 and Appendix X2 of ASTM E3125-17 are designed for periodic or interim assessment of TLSs. But these interim tests also require special targets and a large volume for execution. These requirements can often be limitations for users with limited space or budget. More information on performance testing of TLSs can be found in Muralikrishnan [6].

In response to a need within the forensics community for an interim test that is inexpensive (i.e., requiring no expensive calibrated artifacts or reference instruments), concise (in terms of time needed to execute the test), and flexible (allowing for a variety of testing environments) [7,8], the Crime Scene Investigation and Reconstruction subcommittee (CSIR) of the Organization for Scientific Activities in Forensics (OSAC) [9] is currently developing an interim performance assessment method for TLSs. The procedure involves the measurement of a network of stationary contrast targets from multiple positions of the TLS. There are two parts to the proposed test: Part I evaluates accuracy, while Part II evaluates precision. In Part I, the goal is to compare a few inter-target distances measured using the TLS against a reference value, likely established using a calibrated tape measure. In Part II, the goal is to quantify the precision of the TLS (i.e., the variability along the ranging and angular axes) from measurements of stationary targets from multiple positions of the TLS. More information on Part II can be found in Gregg et al. [7]. In this paper, we explore a technique that uses the TLS under test to establish the reference values for inter-target distances with

* Corresponding author.
E-mail address: balam@nist.gov (B. Muralikrishnan).

https://doi.org/10.1016/j.precisioneng.2026.04.029
Received 14 January 2026; Received in revised form 2 April 2026; Accepted 30 April 2026
Available online 4 May 2026
0141-6359/Published by Elsevier Inc.

low uncertainty, thus obviating the need for even a calibrated tape measure for part I. While this work was driven by a need in the forensics community, we believe this has broader applications, particularly in geodesy and surveying, and in manufacturing and assembly, where performance testing of TLSs and other dimensional measurement equipment is common.

The technique which we employ for this purpose is called self-calibration, and it is well known in the TLS community (see Section 2 for the relevant literature). The primary focus of self-calibration is the estimation of the parameters of a TLS error model to improve its accuracy. We employ this technique with a different objective, i.e., to produce coordinates of the targets, and therefore inter-target distances, with low uncertainty so that these distances may be used as reference values to evaluate the performance of the same TLS or other instruments whose accuracy specifications are larger (typically, by at least a factor of four) than the uncertainties obtained by this method. We explore the technique, discuss its advantages, and highlight its limitations in this paper.

Before we proceed further, we would like to clarify that the term 'self-calibration' as used in this paper does not conform to the definition of calibration in the International Vocabulary of Metrology (VIM3) [10]. Calibration, according to VIM3, is a two-step process. The first step involves establishing a relation between measurement standards and corresponding indications (with uncertainty) and the second step involves using this to determine the result from an indication. Specifically, note 2 in Section 2.39 of VIM3 states that "Calibration should not be confused with adjustment of a measuring system, often mistakenly called "self-calibration", nor with verification of calibration." In our case, we do not use measurement standards and therefore do not perform a true calibration per VIM3. We use the term 'self-calibration' much as a practitioner would in the field, to perform an adjustment of the parameters.

The rest of the paper is organized as follows. We present an overview of related literature in Section 2. We outline the approach, discuss the computational techniques employed, and describe the targets and TLSs used in Section 3. Results from the validation and demonstration experiments are presented in Sections 4 and 5, respectively. Discussion and conclusions are presented in Section 6.

2. Literature review

The process of estimating the parameters of a TLS error model through measurements of a network of stationary targets from multiple TLS positions is referred to as self-calibration. While the focus of our work is not the determination of the model parameters themselves, literature pertaining to self-calibration is indeed relevant. The earliest reported literature in the area of TLS self-calibration is perhaps by Rietdorf et al. [11] and Gielsdorf et al. [12]. They employed a network of planes that were measured from multiple TLS positions to estimate parameters of their error model. Because they used planes, not contrast targets, they were unable to reduce the target to a single point to compute inter-target distances. That was not a concern for them anyway as their objective was to improve the accuracy of their TLS, not to calibrate inter-target distances. Lichti and Franke [13] proposed a self-calibration approach using signalized targets (white circles on a gray background) and demonstrated reduction in the residuals after calibration. Lichti and Licht [14] reported on further studies showing significant improvement in scanner accuracy. Lichti [15] described a comprehensive self-calibration study using signalized targets performed over a period of several months to assess the stability of the error model parameters of their TLS. Using signalized targets would have allowed Lichti to calibrate inter-target distances, but again, that was not their focus. There have since been numerous studies in this area, see Reshetyuk [16] for early discussions on this topic and Refs. [17–25] for subsequent studies. The number and position of the targets, the number of instrument positions, etc., have all been explored in these studies.

The error model employed is an important aspect in ensuring the efficacy of self-calibration. Early studies, such as those by Gielsdorf et al. [12] considered a limited set of parameters such as collimation error, trunnion axis error, and vertical index error. Early self-calibration studies generally relied on the error models developed for theodolites or tacheometers. While TLSs are similar in construction to theodolites, there are some differences. For example, the collimation error is the non-orthogonality between the telescope (collimation axis) and the transit axis. In TLSs, non-orthogonality of the laser beam (collimation axis, *OP* in Fig. A1, Appendix A) with the transit axis (*OT* in Fig. A1, Appendix A) may be due to a tilt in the mirror or a tilt in the laser beam emerging from the source, see Muralikrishnan [6]. This distinction is not clearly highlighted in early literature [15–20,26–28], where it was assumed that mirror tilt is the only cause of the non-orthogonality of the laser beam. In this study, we have used the comprehensive National Institute of Standards and Technology (NIST) error model comprising 15 parameters, proposed by Wang et al. [29], which was based on the 18-parameter model initially proposed by Muralikrishnan et al. [30].

This paper builds on work previously reported by Shi et al. [31] and Icasio-Hernandez et al. [32]. Shi et al. [31] attempted to answer two questions:

1) Are the error model parameters and their uncertainties obtained using a self-calibrated network comparable with those obtained using a network that is calibrated using a reference instrument of higher accuracy?
2) Are the uncertainties in the inter-target distances in the self-calibrated network sufficiently small for the purposes of evaluating the performance of the TLS? That is, how do the uncertainties compare against maximum permissible error specifications of the instrument under test?

On the other hand, Icasio-Hernandez et al. [32] attempted to use a self-calibrated network to quantify uncertainty in measurements made using a laser tracker. While we adopt the self-calibration technique in Shi et al. [31] and the model-fitting approach in Icasio-Hernandez et al. [32], we attempt to answer a different set of questions:

1) How small are the errors in the inter-target distances calculated by this technique when compared to measurements made from a single position of the TLS?
2) Are the uncertainties in the inter-target distances calculated by this technique realistic, i.e., are the observed errors smaller than the calculated uncertainties?
3) Does the technique apply to both a short-range high accuracy and a long-range low accuracy TLS?
4) What, if any, are the limitations of this technique?

3. Materials and methods

3.1. Approach

We placed checkerboard targets in a room so that they were well distributed, covering as large a range of the horizontal and vertical angle encoders as possible. We identified four positions in the room where the TLS could be placed so that the angle of incidence to the targets was between 5° and 45° for all targets from all positions [33]. We placed the TLS as low as possible on the stand for two of the positions and as high on the stand as possible for the remaining two positions, to increase the range of angles on the vertical angle encoder. We rotated the TLS by 90° between positions to cover the full range of horizontal angles. With the TLS at the first position, we scanned all targets in the front-face and extracted centers using the procedure described in Rachakonda et al. [34]. With the TLS still at the same position, we scanned all targets in the back-face and extracted centers. As we will show later, the ability to scan targets separately in front-face and in back-face is critical for implementing this technique. We repeated this process for the other TLS positions. Finally, we performed a least-squares bundle adjustment to calculate the composite center coordinates (i.e., average from the four TLS positions). The bundle adjustment can be performed with or without fitting the error model of the TLS; however, incorporating the error model of the TLS is an essential part of self-calibration.

The bundle adjustment produces not only the composite center coordinates for all targets but also a measure of the TLS's intrinsic errors captured as the standard deviation along the range and angular axes directions. The inter-target distances can be calculated from the composite center coordinates while the uncertainty in those distances can be computed from a Monte Carlo simulation (MCS) using the TLS's intrinsic errors. We describe the calculation process in more detail in the next section. Fig. 1 shows a schematic of 20 targets (distributed across three walls) measured from four positions of the TLS.

While the calculation of the composite center coordinates is described in Section 3.2, we provide a brief explanation for purposes of clarity. If repeated scans of a target are acquired from a single TLS position and the center coordinates are calculated from each scan, the average center coordinates can be calculated easily, i.e., through a simple arithmetic averaging process. Such arithmetic averaging is not possible if the TLS position is moved between the scans. In order to estimate the target center coordinates that effectively averages the four scans (one scan from each of the four TLS positions), we perform a mathematical rotation and translation of the coordinate systems for TLS positions 2, 3, and 4, so that the target centers acquired from those positions overlap with that acquired from position 1, to the extent possible. Because the targets centers are now in the coordinate system of TLS at position 1, we may now perform a simple arithmetic averaging to obtain the ‘average target center coordinates’. We refer to this average as the composite center coordinates. The rotation and translation process mentioned earlier is the core of the bundle adjustment process.

Clearly, including more TLS positions and targets will improve the accuracy of the inter-target distances. We chose four TLS positions and 20 targets as a compromise between the desire for high accuracy and the time taken to acquire and process the data. The targets themselves must be well distributed spatially to achieve the best results; using all available walls, the floor and the ceiling is ideal. However, obstructions and other physical constraints, including the inability to orient the target to meet the angle of incidence requirements, limited the positioning of targets.

In this paper, we report the results from two sets of experiments, a validation experiment and a demonstration experiment. The validation experiment, described in Section 4, used a laser tracker (an instrument that can provide substantially higher accuracy than a TLS) to establish the validity of our proposed approach. We employed a specialized contrast target that can be mounted on a laser tracker nest for this experiment. The demonstration experiment, described in Section 5, used paper targets fixed on walls. Because a laser tracker cannot be used to establish the reference coordinates, we simply compared the results from the two TLSs that we used for this study.

3.2. Data processing

We describe the calculation of the composite coordinates and the uncertainty in the inter-target distances in this section. We first describe the bundle adjustment process without fitting the TLS error model in Section 3.2.1. This is based on the work described by Calkins [35] in his dissertation. We then describe the process of including the TLS error model in the bundle adjustment process in Section 3.2.2; this constitutes the main contribution of this paper. We describe the calculation of the uncertainty in the inter-target distances in Section 3.2.3.

3.2.1. Bundle adjustment, no error model fitting

Suppose a set of n targets are measured from m TLS positions. We calculate the composite coordinates of the targets through a bundle adjustment process as described here. Let $C_{f\,j}$ represent the Cartesian coordinates of the targets measured from position j in the front-face of the TLS. $C_{f\,j}$ is a matrix of size $n \times 3$, where the ith row has the center coordinates $\left(x_{i,j}, y_{i,j}, z_{i,j}\right)$ of the ith target. Let $S_{f\,j}$ represent the spherical coordinates of the targets measured from position j (i.e., corresponding to the Cartesian coordinates $C_{f\,j}$). $S_{f\,j}$ is also a matrix of size $n \times 3$, where the ith row has the center coordinates $\left(r_{i,j}, \theta_{i,j}, \varnothing_{i,j}\right)$ of the ith target, where r is the range to the target, and θ and $\varnothing$ are the horizontal and vertical angles to the target, respectively. Let $C_{b\,j}$ represent the Cartesian

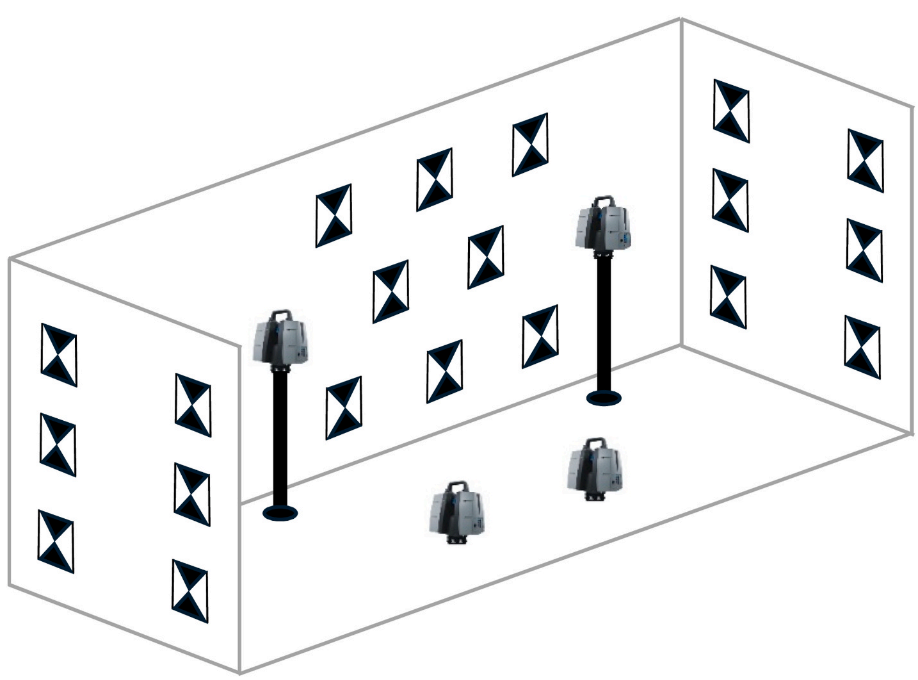

Fig. 1. Schematic showing targets in a room and four positions of the TLS. The target and TLS positions shown are for illustration purposes only, as these do not represent the actual positioning in our experiments.

coordinates of the targets measured from position j in the back-face of the TLS and $S_{b,j}$ represent the corresponding spherical coordinates.

Let R_j represent the rotation matrix and T_j represent the translation vector for transforming the measured coordinates from the jth frame to the first frame (i.e., the coordinate frame associated with position 1). The rotation matrix R_j is the product of rotation matrices about three orthogonal axes and is given by

$$R_j = R_{x,j} R_{y,j} R_{z,j}, \tag{1}$$

where

$$R_{x,j} = \begin{pmatrix} 1 & 0 & 0 \\ 0 & \cos\alpha_j & \sin\alpha_j \\ 0 & -\sin\alpha_j & \cos\alpha_j \end{pmatrix}, \tag{2}$$

$$R_{y,j} = \begin{pmatrix} \cos\beta_j & 0 & \sin\beta_j \\ 0 & 1 & 0 \\ -\sin\beta_j & 0 & \cos\beta_j \end{pmatrix}, \text{ and} \tag{3}$$

$$R_{z,j} = \begin{pmatrix} \cos\gamma_j & -\sin\gamma_j & 0 \\ \sin\gamma_j & \cos\gamma_j & 0 \\ 0 & 0 & 1 \end{pmatrix}. \tag{4}$$

In Eqs. (2)–(4) above, $\alpha_j, \beta_j,$ and γ_j represent rotation angles about the x, y, and z axes, respectively. The translation vector is given by

$$T_j = \begin{pmatrix} t_{x,j} \\ t_{y,j} \\ t_{z,j} \end{pmatrix}, \tag{5}$$

where $t_{x,j}, t_{y,j},$ and $t_{z,j}$ represent translation along the x, y, and z axes, respectively. Note that $\alpha_j, \beta_j, \gamma_j, t_{x,j}, t_{y,j},$ and $t_{z,j}$ are scalar quantities, R_j is a matrix of size 3 × 3, and T_j is a vector of size 3 × 1. Without loss of generality, we can assume the coordinate system at the first TLS position as the reference for all calculations, thus $\alpha_1 = \beta_1 = \gamma_1 = t_{x,1} = t_{y,1} = t_{z,1} = 0$. With m positions, there are 6(m – 1) unknown rotation and translation parameters.

Let $\overline{C}_1$ represent the 3n unknown composite Cartesian coordinates in frame 1 (subscript 1 indicates the frame). The composite coordinates transformed to frame j (indicated by the superscript) are given by

$$\overline{C}_1^j = R_j^{-1}(\overline{C}_1 - T_j). \tag{6}$$

Let $\overline{S}_1^j$ be the composite spherical coordinates corresponding to the composite Cartesian coordinates $\overline{C}_1^j$. Then the front-face and back-face residuals can be calculated as follows:

$$f_{f,j} = S_{f,j} - \overline{S}_1^j. \tag{7}$$

$$f_{b,j} = S_{b,j} - \overline{S}_1^j. \tag{8}$$

Note that $f_{f,j}$ and $f_{b,j}$ are matrices of size n × 3. We reshape the matrices to vectors of size 1 × 3n. If we only consider front-face data, we minimize the sum of squared residuals $F = \left[f_{f,1}\, f_{f,2} \ldots f_{f,m}\right]$ to find all 6(m – 1) + 3n unknown parameters. If we only consider back-face data, we minimize the sum of squared residuals $F = \left[f_{b,1}\, f_{b,2} \ldots f_{b,m}\right]$ to find all 6(m – 1) + 3n unknown parameters. If we consider both front-face and back-face data, we minimize the sum of squared residuals $F = \left[f_{f,1}\, f_{f,2} \ldots f_{f,m}\, f_{b,1}\, f_{b,2} \ldots f_{b,m}\right]$ to find all 6(m – 1) + 3n unknown parameters. Note however that the residuals are all not in the same units. Residuals along the ranging direction are in units of length while the residuals along the angular axes are in units of angle. To ensure uniformity in units, we scale the residuals along the angular axes by the composite range, so all residuals are in units of length.

The following points are worth emphasizing:

- The coordinate system of the TLS at position 1 is chosen as the reference, that is, the composite coordinates are calculated in that frame. The choice of which position to use is arbitrary, this does not affect the bundle-adjustment process.
- The residuals can only be calculated in the frame of the TLS at each position because the residuals are in spherical coordinates, and they make physical sense only in the coordinate system of the TLS. Because the composite coordinates are defined in frame 1, we must transform them to the frame corresponding to each TLS position before we can calculate the residuals, as shown in Eq. (6).

The computational process is illustrated in Fig. 2. Part (a) shows the measurement of the targets from different positions (two-dimensional data for illustration purposes), (c) shows the transformation of the composite coordinates to the individual frames, and (d) shows the calculation of the residuals for one target. We ignore part (b) in this section because we are not fitting the TLS error model in this case.

We can further improve the target composite coordinate accuracy by weighting the residuals as described by Calkins [35]. This is done iteratively, by calculating the standard deviation of the residuals along the ranging and angular axes directions at the end of the bundle-adjustment and then using the inverse of those values as the weights for the next iteration, repeating this process until the weights do not change significantly.

3.2.2. Bundle adjustment with error model fitting

In the preceding subsection, we only needed to estimate the 6(m-1) rotational and translational parameters and the 3n unknown composite coordinates. We can add a layer of complexity to the computational process by also fitting the error model of the TLS. The error model is a function of the measured spherical coordinates and some scalar parameters. These parameters capture the mechanical and optical misalignments in the TLS, such as non-orthogonality of the horizontal and vertical axes, the tilt in the laser beam, etc. The error model used here is described in Ref. [29] and has 15 scalar parameters. We briefly describe the error model in the appendix for completeness.

Let $\overline{C}_1$ represent the composite coordinates in frame 1. The composite coordinates transformed to frame j are given by

$$\overline{C}_1^j = R_j^{-1}(\overline{C}_1 - T_j). \tag{9}$$

Let $\overline{S}_1^j$ be the composite spherical coordinates corresponding to the composite Cartesian coordinates $\overline{C}_1^j$. As before, let $S_{f,j}$ and $S_{b,j}$ represent the spherical coordinates of the targets measured from position j in the front-face and back-face of the TLS, respectively. Given estimates of the 15 model parameters G (a vector of size 15 × 1), the corrected spherical coordinates at the jth position, S_j^c, can be computed from the error model E as

$$S_{f,j}^c = E(S_{f,j}, G). \tag{10}$$

$$S_{b,j}^c = E(S_{b,j}, G). \tag{11}$$

Then the front-face and back-face residuals can be calculated as

$$f_{f,j} = S_{f,j}^c - \overline{S}_1^j \tag{12}$$

$$f_{b,j} = S_{b,j}^c - \overline{S}_1^j \tag{13}$$

Note that $f_{f,j}$ and $f_{b,j}$ are matrices of size n × 3. We reshape the matrices to vectors of size 1 × 3n. Our objective is to minimize the sum of squared residuals $F = \left[f_{f,1}\, f_{f,2} \ldots f_{f,m}\, f_{b,1}\, f_{b,2} \ldots f_{b,m}\right]$ to find all unknown parameters. As before, to ensure uniformity in units, we scale the residuals along the angular axes by the composite range, so all residuals are in units of length.

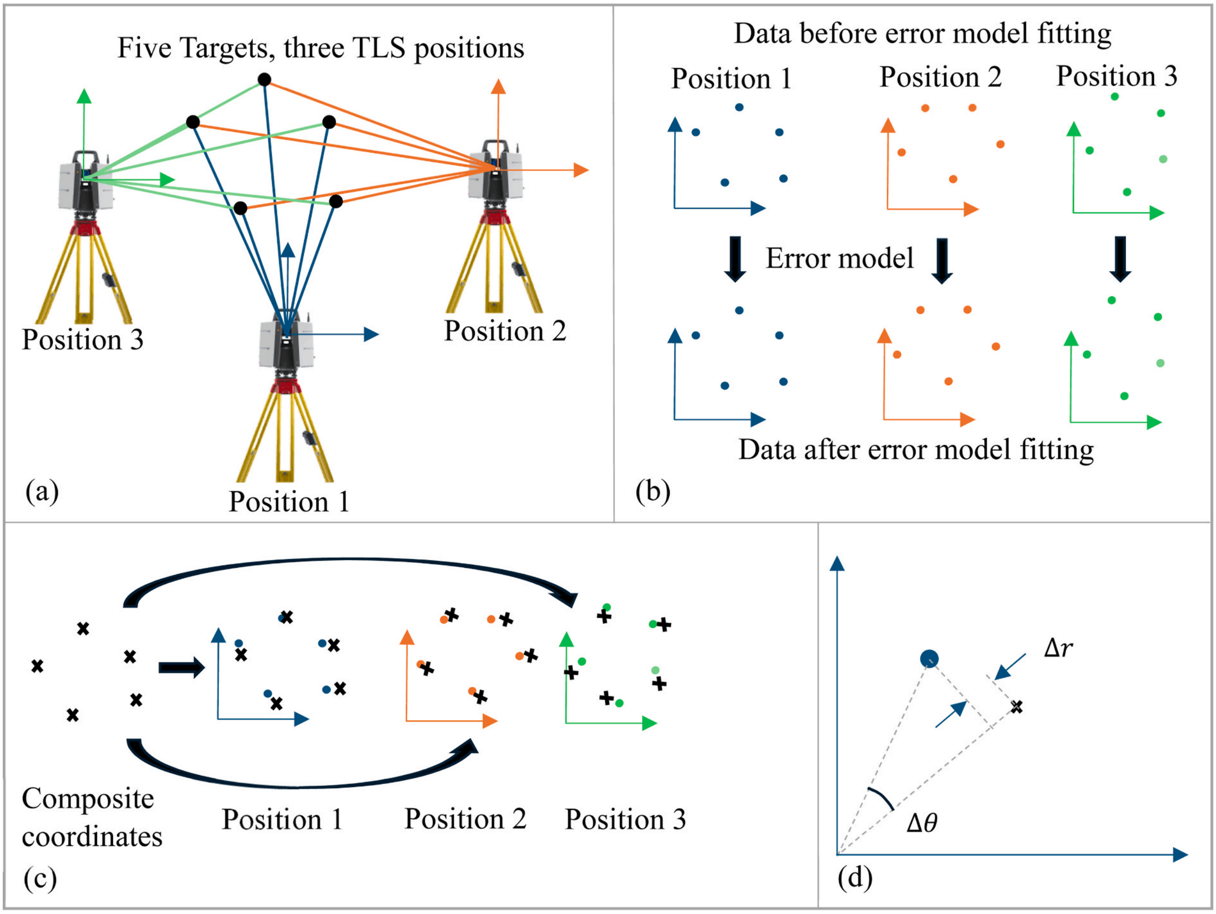

Fig. 2. Process of transforming composite coordinates to individual measurement frames and calculation of the residuals, (a) showing the measurement of five targets from three positions of the TLS, (b) fitting the error model of the TLS (this part is not applicable to Section 3.2.1), (c) the transformation of the composite coordinates to the individual frames, and (d) calculation of the residuals for one target in the frame in which it was collected.

The computational process is illustrated in Fig. 2. Parts (a), (c) and (d) are the same as in the preceding section. Part (b) is the additional step and shows the correction of the measured data using estimates of the error model parameters. As before, we can further improve the target composite coordinate accuracy by weighting the residuals as described by Calkins [35].

3.2.3. Uncertainty calculation

Bundle adjustment, whether we fit the TLS error model or not, aims to reduce the residuals along the ranging and angular directions. The standard deviations of these residuals are a measure of the TLS intrinsic errors, which we can then use to estimate the uncertainty of any measured point coordinate or other derived features such as the distances between points. Fig. 3 (a) and (b) show a flowchart and an illustration of the uncertainty calculation process. Through a Monte Carlo Simulation (MCS), we propagate these standard deviations through the bundle adjustment computational process (as described in Section 3.2.1 if we do not fit the TLS error model, and in Section 3.2.2 if do fit the model) to calculate the standard deviation in the inter-target distances. Specifically, for each iteration of the MCS, we perturb the measured point coordinates (all n targets from m positions), perform the bundle adjustment, calculate the composite coordinates, and the distances between all composite coordinate pairs. We repeat this process 1000 times as shown in Fig. 3(a). At the end of the repeats, for each composite coordinate pair, we calculate the standard deviation of the 1000 distance values. We consider this standard deviation as the standard uncertainty for that distance. However, there are several additional factors to consider, as discussed in Section 6. Note that we did not consider the correlation between the three directions when performing the MCS; independent draws from the distributions along the three directions were propagated in the MCS.

3.3. TLSs and targets used

Two TLSs were considered in this study, a short-range, high-accuracy TLS (TLS A) and a long-range, lower-accuracy TLS (TLS B). The short-range TLS had a range of about 20 m, range noise of about 0.1 mm at 3 m, and maximum angular point density of 90 points-per-degree (ppd). The long-range TLS had a range of over 1 km, range noise of about 0.4 mm at 10 m, and maximum angular point density of 218 ppd. The internal error model of TLS A was turned off for the experiments so that the instrument was at its worst-performance condition. This was intentionally done to demonstrate the validity of our technique even with a fully uncompensated TLS. The internal error model of TLS B could not be turned off, we therefore performed the experiments with the internal model turned on.

The contrast target employed for the validation experiment was about 100 mm × 50 mm in size and had a partial 38.1 mm (1.5 in) diameter sphere on the backside, see Fig. 4. We had six such targets available for this experiment. The targets were designed so that the center of the partial sphere in each target coincided with the center of the target on the front face allowing for the interchangeability between the target and a spherically mounted retro-reflector (SMR). Although designed to be nominally coincident, the optical (as determined by the TLS) and mechanical (center of the partial sphere) centers might be offset. This offset may be resolved into an in-plane (in the plane of the

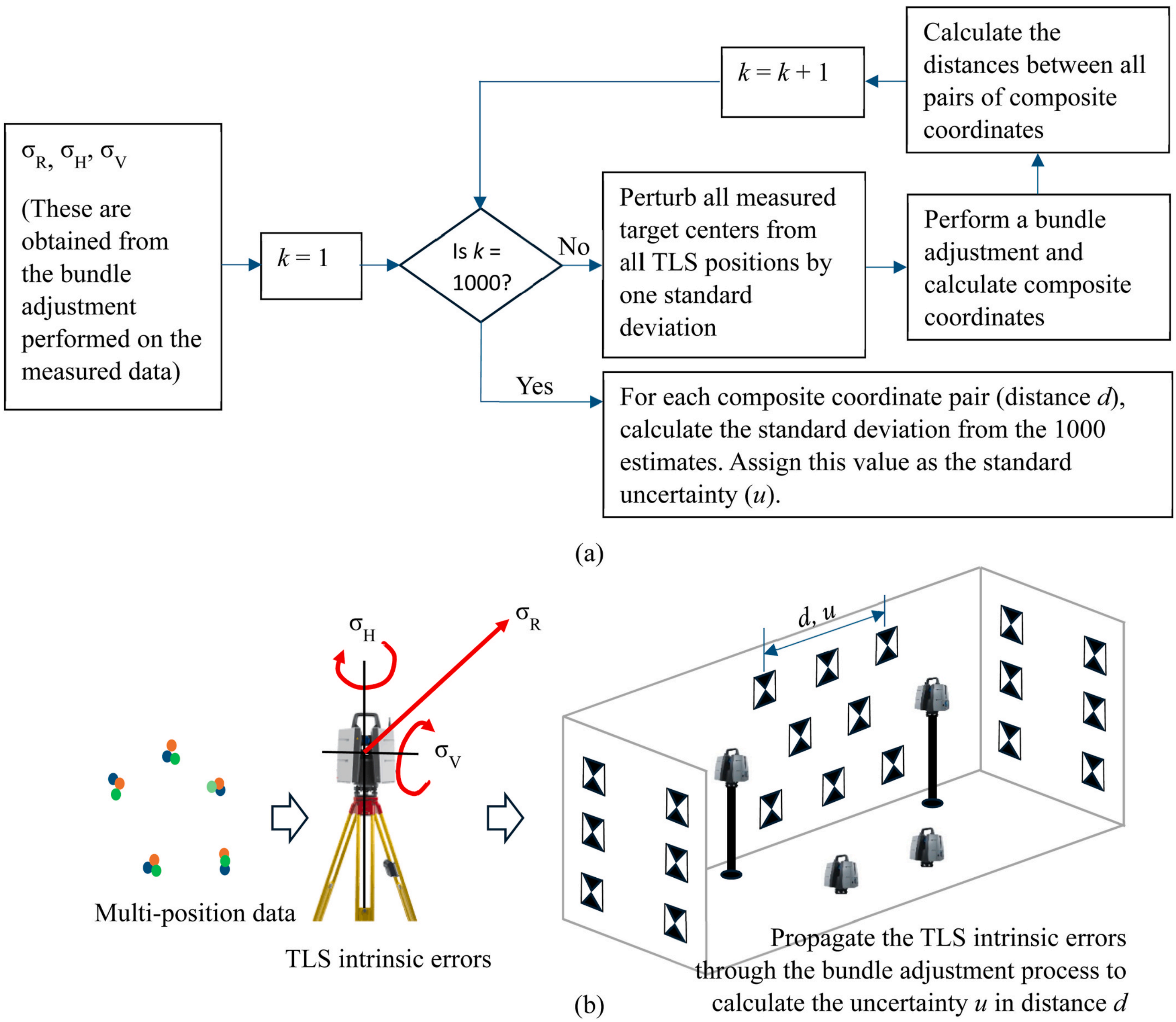

Fig. 3. (a) Flow chart showing the calculation of the distance uncertainty through an MCS, (b) pictorial representation of the same.

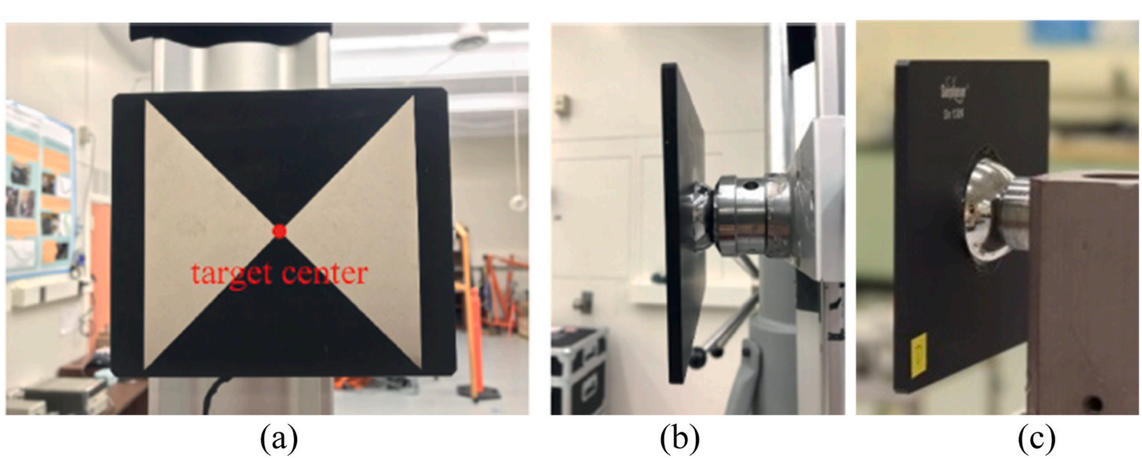

Fig. 4. Different views of the contrast target, (a) front face showing the target center, (b) side view showing the partial sphere and the SMR nest, and (c) back view showing the partial sphere and SMR nest.

target) eccentricity and an out-of-plane eccentricity. We did not measure the in-plane eccentricity. Instead, we attenuated the effect of any in-plane eccentricity by performing two scans, once with the target in a certain orientation, and once after rotating the target by 180° about its surface normal vector, then averaging the centers. To reduce the effect of any out-of-plane eccentricity between the optical and mechanical centers, the eccentricity of all six targets were measured on a Cartesian coordinate measuring machine (CMM) with a maximum permissible error specification of 0.5 + 0.7 μm/m. A 38.1 mm (1.5 in) SMR nest was mounted on the table of the CMM. A 38.1 mm (1.5 in) steel sphere was placed on the nest, 29 points were acquired on the sphere using the contact probe, and the sphere center determined through a least-squares fitting process. The coordinate system was translated so that the sphere center was the new origin. The sphere was replaced by the target with its face nominally horizontal. The table and the bridge were moved so that the probe was located at $x = 0$ and $y = 0$. The probe was driven along the negative Z direction and the point on the surface of the target was recorded. The difference between this point (after correcting for probe radius) and the sphere center was recorded as the out-of-plane offset. We measured this offset for all six targets. The average was determined to be 0.05 mm (with a standard deviation of 0.005 mm), and all range measurements by both TLSs were corrected for this offset.

The contrast target employed for the demonstration experiment was about 203.2 mm × 203. 2 mm (8 in × 8 in) in size and printed on cardstock using a laser printer, see Fig. 5. We printed 20 such targets. The black portion of the target was printed at the maximum gray scale intensity possible. Magnetic-adhesive sheets were procured, the adhesive side was fixed to the back of the target while the magnetic side was fixed to the walls in the laboratory. To ensure uniformity between TLSs, the center of the contrast target in the TLS scans (for targets shown in both Figs. 4 and 5) were determined using the procedure described by Rachakonda et al. [34] for both TLSs.

4. Validation experiment

The purpose of the validation experiment was to demonstrate the applicability of this technique by comparing the results against a more accurate instrument, the laser tracker. We describe the experiment and results in this section.

4.1. Experimental setup

The validation experiment was performed in a 11 m × 6 m × 3 m space. Twenty laser tracker nests were placed on stands and on the floor so that they were roughly on three orthogonal planes. An SMR was placed in each nest. The center coordinates of the SMRs were measured using a laser tracker. To improve measurement accuracy, the center coordinates were measured in the front-face and again in the back-face of the laser tracker, and the results were averaged. Furthermore, measurements were performed from four locations of the laser tracker, and the composite coordinates were calculated as described in Section 3.2.1. Following the laser tracker measurements, the SMRs were removed, and a contrast target was mounted on each nest. All 20 targets were scanned in the front-face and again in the back-face from each of the four TLS positions. Because we only had six contrast targets available, we placed a target in each of six nests, performed the scans, moved the targets to the next set of nests, and repeated the process. The data were then processed as described in Sections 3.2.1, 3.2.2, and 3.2.3. Fig. 6 shows the relative location of the targets and TLSs.

4.2. Ranging errors in the TLSs

For each of the four TLS positions, we have 20 front-face center coordinates and 20 back-face center coordinates. We can compute a total of 190 inter-target (i.e., between target pairs 1-2, 1-3, 1-4, …, 18-19, 18-20, and 19-20) distances from 20 center coordinates. The errors in these 190 distances (with respect to the laser tracker) are shown in Fig. 7(a), separately for the front-face and back-face measurements, for one position of TLS A. These errors are large, on the order of about ±3 mm, because the internal error model of the TLS was turned off. Fig. 7(b) shows the corresponding errors for one position of TLS B. There is a clear linear trend in Fig. 7(b), indicating the presence of a ranging error in TLS B. Such a trend is not evident in Fig. 7(a) for TLS A.

To verify that the observed linear trend is in fact due to errors in the ranging unit of the TLS, we performed a ranging test on TLS B. For purposes of completeness, we also performed the same ranging test on TLS A. These tests were performed using the contrast target shown in Fig. 4 and a laser tracker as a reference instrument. The laser tracker and the TLS under test were placed adjacent to each other, as shown in Fig. 8(a). A stand with a 38.1 mm (1.5 in) nest was placed about 3.5 m from the TLS. An SMR was placed in the nest and its center coordinate was

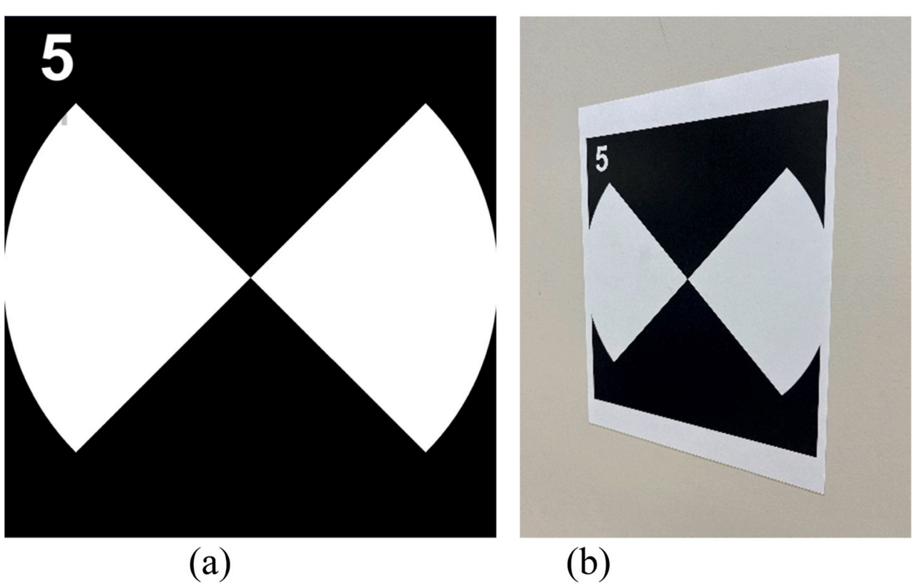

Fig. 5. (a) Contrast target drawing prior to printing, (b) as printed on cardstock, fixed to adhesive/magnetic sheet, and attached to the wall for the demonstration experiment.

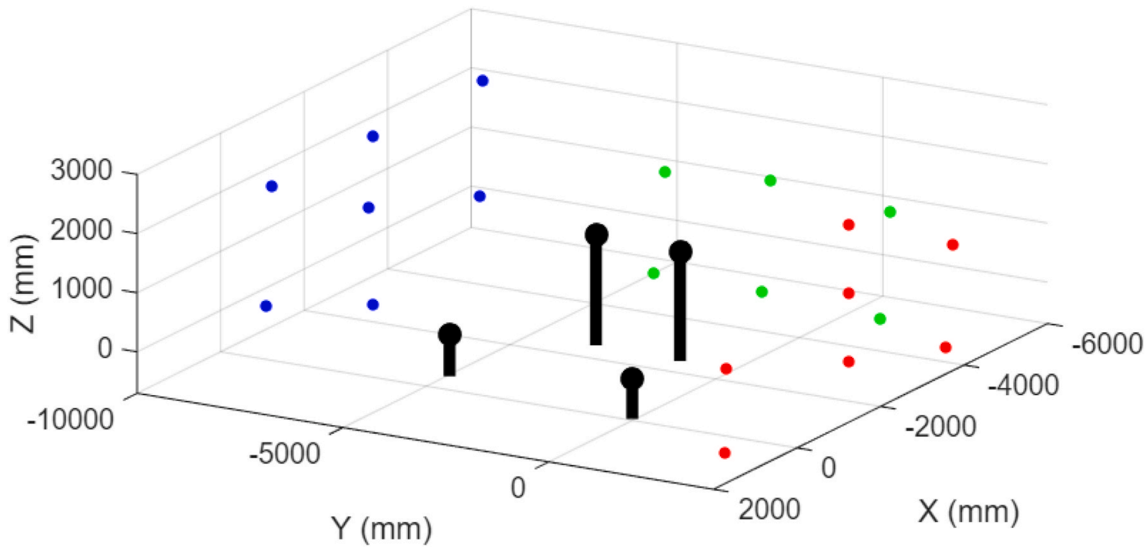

Fig. 6. Target and TLS locations in the validation experiment. The TLSs are shown in black. The seven targets shown in blue, the seven shown in red, and the six shown in green are each nominally on a plane. (For interpretation of the references to colour in this figure legend, the reader is referred to the Web version of this article.)

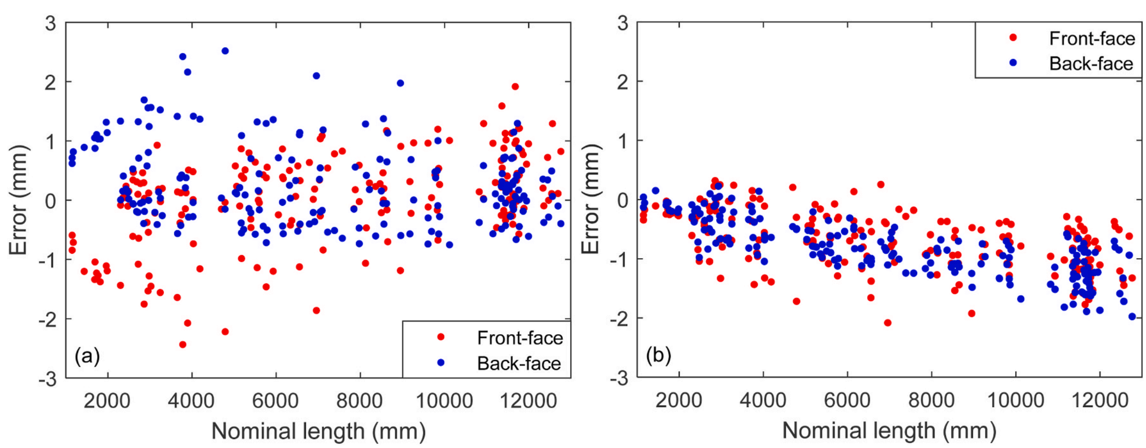

Fig. 7. (a) Inter-target distance errors for position 1 of TLS A, (b) inter-target distance errors for position 1 of TLS B indicating the presence of a linear (slope) error.

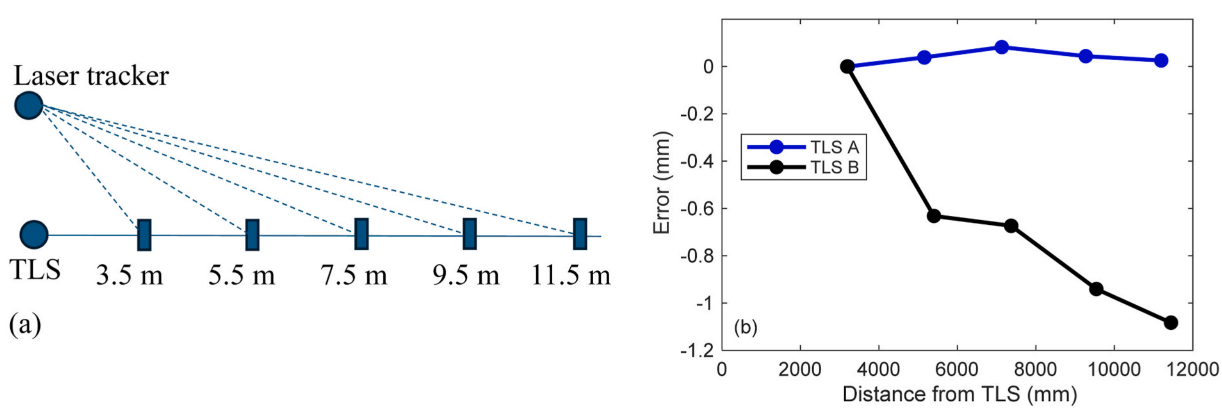

Fig. 8. (a) Ranging error test setup schematic (top view shown), (b) TLS ranging errors.

measured using the laser tracker. The SMR was then removed, a contrast target was placed in the same nest, the TLS performed a scan, and the target center coordinate was computed from the scan data. The stand was then moved to the other positions along a line with the TLS and the first position, and the process was repeated. For both the laser tracker and the TLS, distances were computed with respect to the first position, and ranging errors were calculated. These errors are shown in Fig. 8(b). TLS A does not show any noticeable slope, whereas a clear slope is visible for TLS B, about 0.1 mm/m. All range measurements performed by TLS B were corrected using this scale factor prior to performing the computations described in Section 3. The linear ranging error in TLS B, if uncorrected, constitutes a critical limiting factor in achieving small uncertainties with our technique. We discuss this further in Section 6.

4.3. Angular errors in the TLSs

As mentioned earlier, for each of the four TLS positions, we have 20 front-face center coordinates and 20 back-face center coordinates, for a total of 80 front-face and 80 back-face coordinates. We converted the coordinates from Cartesian to spherical and calculated the difference between the front-face and back-face horizontal angle, $\Delta\theta$, and vertical angle, $\Delta\varnothing$. We multiplied these angular differences with the range r (the average of the front-face and back-face range values) and plotted them as a function of horizontal angle θ and vertical angle $\varnothing$, as shown in Fig. 9. It is clear from the figure that the scaled differences $\Delta\theta$ and $\Delta\varnothing$ are a function of the vertical angle $\varnothing$ for both TLSs, although for TLS A, the differences are much larger because the TLS is uncompensated. Such large differences indicate the presence of systematic angular errors that can be compensated by the geometric error model, as we will show later.

4.4. Errors in the inter-target distances calculated from the composite coordinates

Fig. 10(a) shows the errors in the 190 inter-target distances for one position of TLS A; it is the same plot as in Fig. 7(a), shown here again for reference. Fig. 10(b) shows the error in the inter-target distances at each of the four TLS positions after averaging the front-face and back-face coordinates. The errors are substantially smaller, about ±1 mm for the longest lengths, due to averaging of the systematic errors which change sign between the front-face and back-face. Note that the errors shown in Fig. 10 correspond to the raw data, i.e., the data as measured, prior to the computation of composite coordinates described in Section 3.

We next present the errors in the 190 inter-target distances calculated from the composite coordinates. We consider three cases, described below:

- Case I: Composite coordinates calculated using only the front-face data from each of the four TLS positions, simple rigid body transform, no TLS error model fitting, per Section 3.2.1. This is a simplistic averaging approach expected to result in larger distance errors.
- Case II: Composite coordinates calculated using both the front-face and back-face data from each of the four TLS positions, simple rigid body transform, no TLS error model fitting, per Section 3.2.1. This is a better approach and expected to result in lower distance errors.
- Case III: Composite coordinates calculated using both the front-face and back-face data from each of the four TLS positions, rigid body transform with TLS error model fitting, per Section 3.2.2. This is the approach we advocate in this paper and is expected to produce the smallest distance errors.

Fig. 11(a) shows the errors in the 190 inter-target distances for Case I. The errors are large, about ±2.5 mm. Fig. 11(b) shows the errors in the 190 inter-target distances for Case II. The errors are within ±1 mm. These are smaller than those in Case I because averaging the front-face and back-face coordinates attenuates the effect of several systematic errors in the TLS. Fig. 11(c) shows the errors for Case III. The errors drop significantly to within ±0.15 mm. These errors are at least 20 times smaller than the distance errors from any single TLS position (Fig. 10 (a)), thus, a significant improvement is achieved through our model-

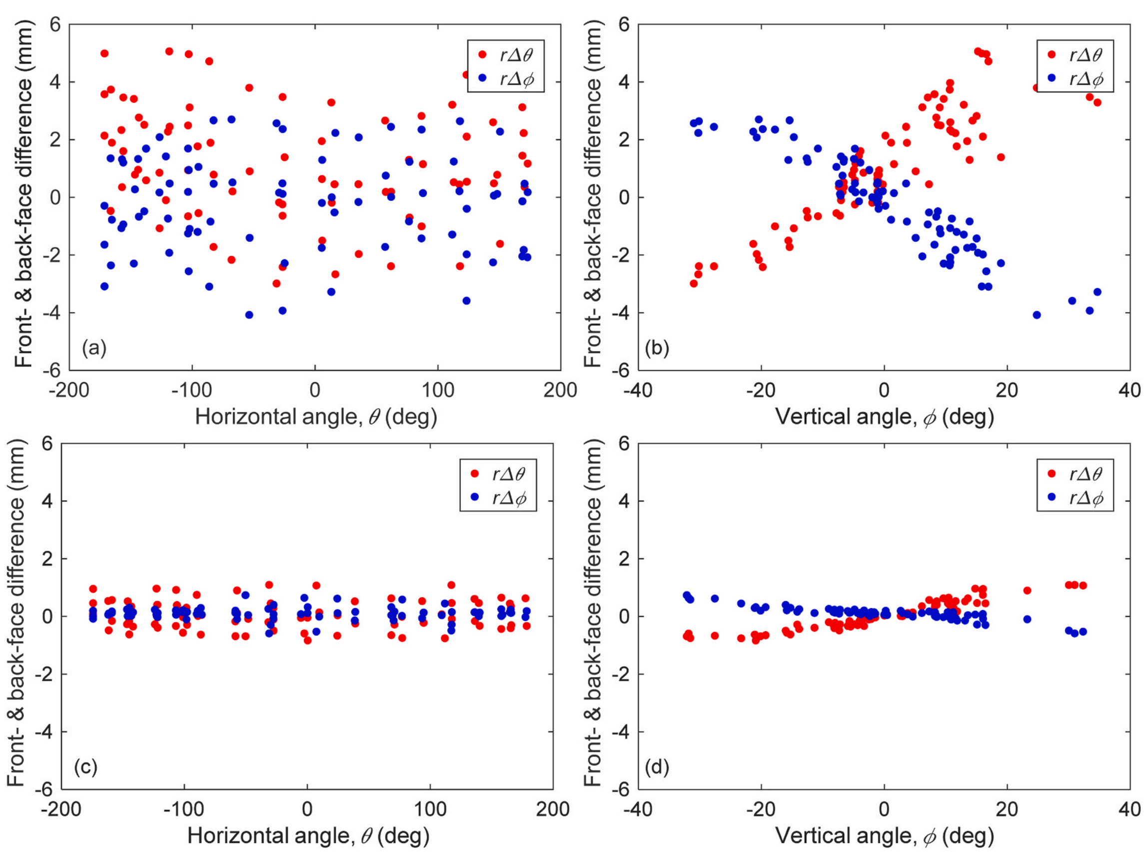

Fig. 9. Difference between the scaled front-face and back-face horizontal angle, $r\Delta\theta$, and vertical angle, $r\Delta\varnothing$ for TLS A as a function of (a) horizontal angle θ and (b) vertical angle $\varnothing$. Difference between the scaled front-face and back-face horizontal angle, $r\Delta\theta$, and vertical angle, $r\Delta\varnothing$ for TLS B as a function of (c) horizontal angle θ and (d) vertical angle $\varnothing$.

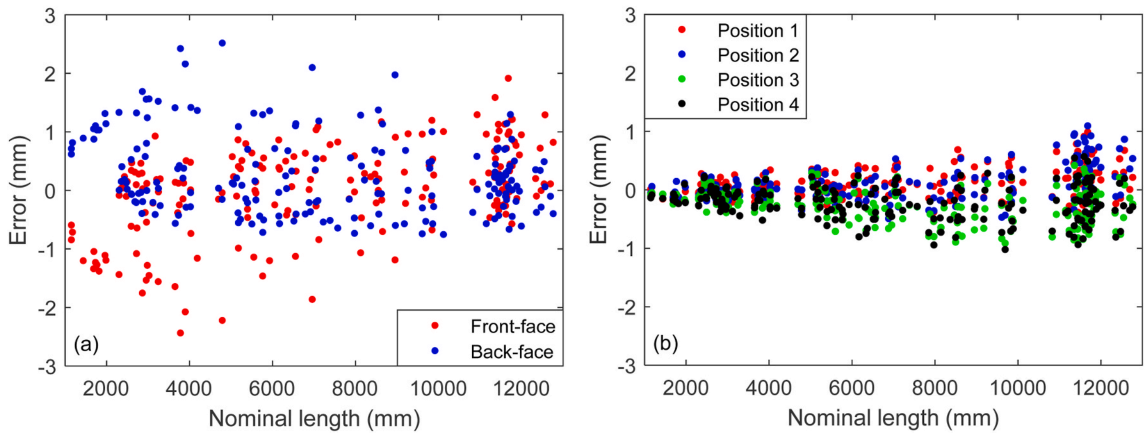

Fig. 10. (a) Inter-target distance errors for position 1 of TLS A, (b) inter-target distance errors at each of the four TLS positions after averaging front-face and back-face data.

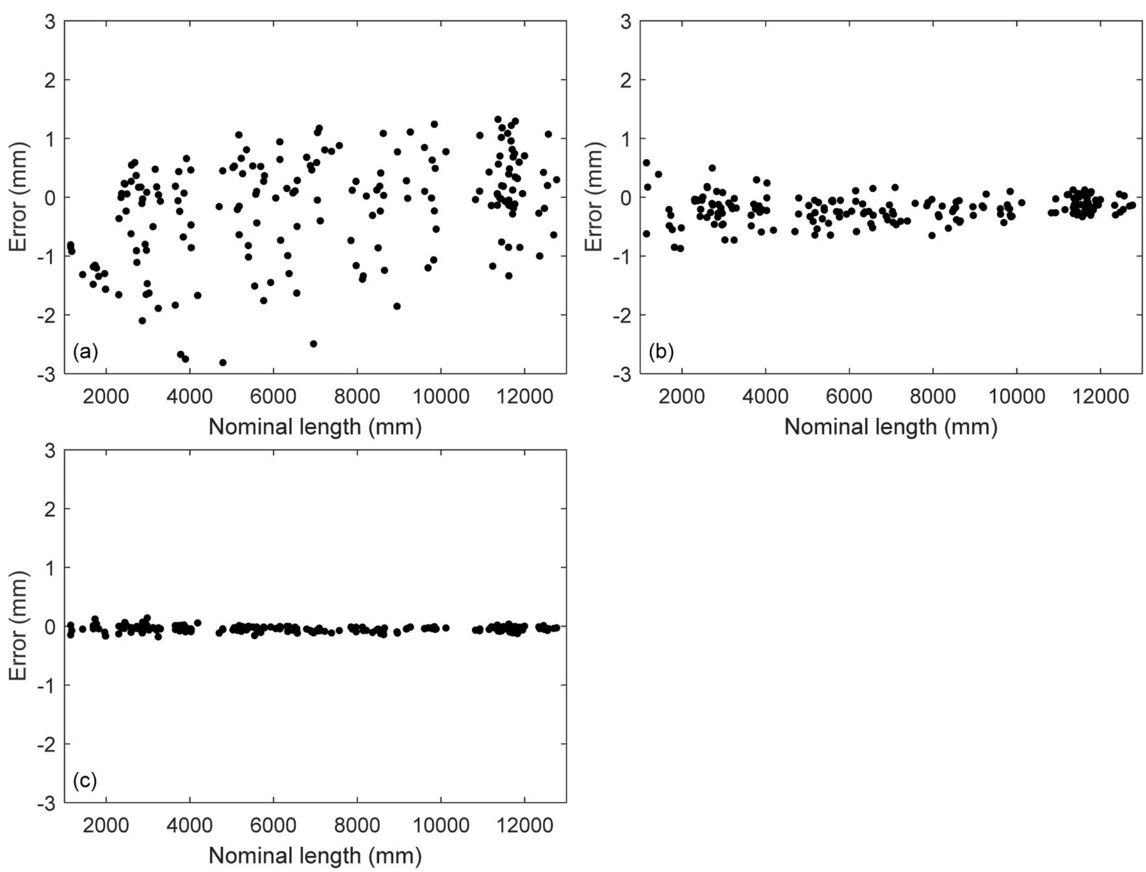

Fig. 11. TLS A inter-target distance errors for (a) Case I, (b) Case II, and (c) Case III.

fitting approach.

Similar plots as above are shown in Figs. 12 and 13 for TLS B. Fig. 12(a) shows the errors in the 190 distances for one position of the TLS A, after correcting for the slope seen in Fig. 8(b). The errors are within about ±1.25 mm. Fig. 12(b) shows the error in the inter-target distances at each of the four positions after averaging the front-face and back-face coordinates. The errors are within about ±1 mm. Note that the errors shown in Fig. 12 are for the raw data, i.e., the data as measured, prior to the computation of composite coordinates as described in Section 3.

Fig. 13(a) shows the errors in the 190 inter-target distances for Case I. The errors are within about ±1 mm. Fig. 13(b) shows the errors in the 190 inter-target distances for Case II. The errors are within about ±0.5 mm, lower than in Case I as expected. Finally, Fig. 13(c) shows the errors in the 190 inter-target distances for Case III. The errors drop significantly to within ±0.25 mm. These errors are at least 5 times smaller than the distance errors from any one position of the TLS (Fig. 12(a)), thus, a significant improvement is achieved through our model-fitting approach.

4.5. Uncertainty versus errors

The bundle adjustment process described in Section 3.2 not only resulted in composite coordinates for the targets but also estimates of the intrinsic instrument errors, as described by the standard deviation along

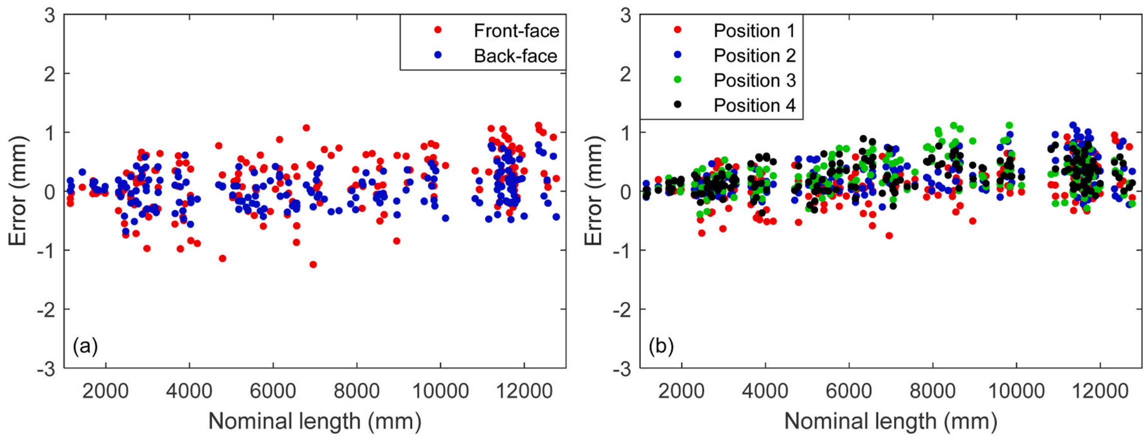

Fig. 12. (a) Inter-target distance errors for position 1 for TLS B, (b) inter-target distance errors at each of the four TLS positions after averaging front-face and back-face data.

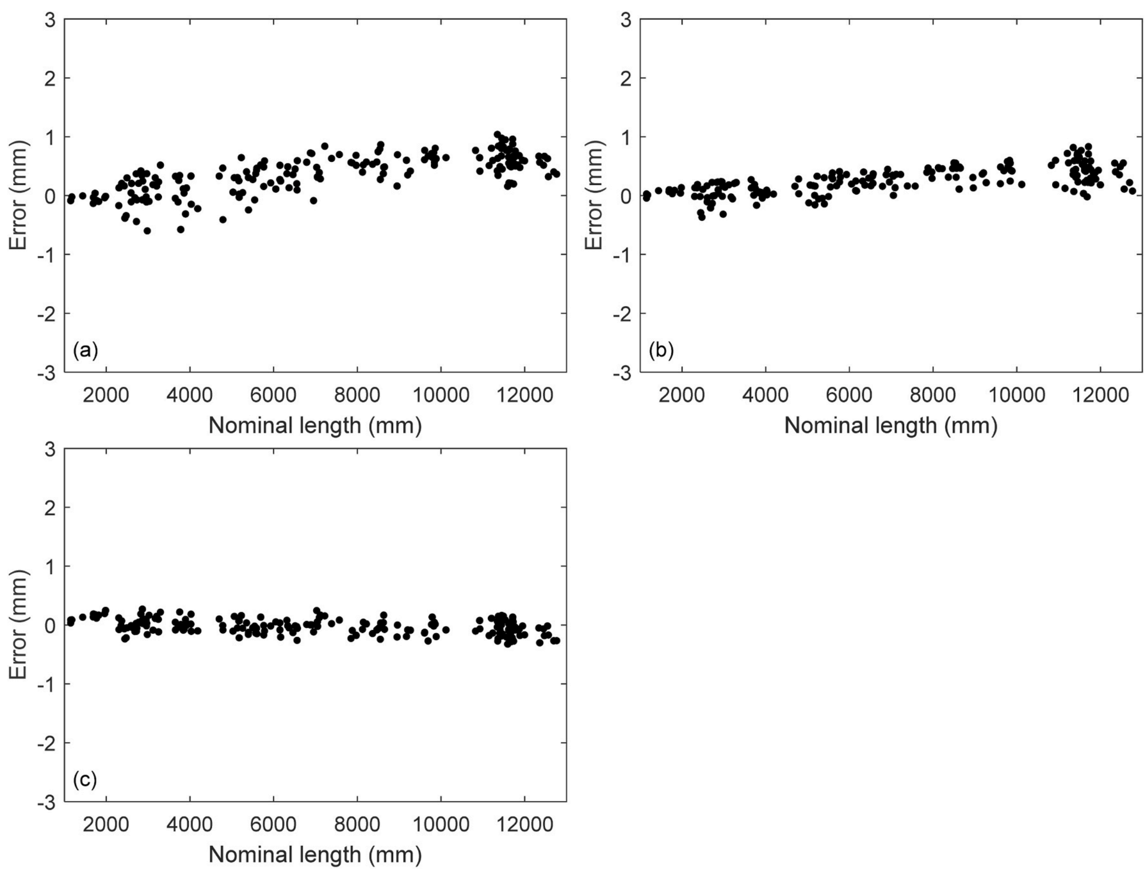

Fig. 13. TLS B inter-target distance errors for (a) Case I, (b) Case II, and (c) Case III.

the ranging and angular axes directions. These standard deviations are listed in Table 1 for TLS A for the three cases. We propagated the values listed in the table through an MCS to estimate the uncertainty in the inter-target distances for each of the cases. The range of the uncertainties for the 190 distances for each case is also listed in Table 1. We assess the validity of these uncertainties by comparing them to the measured errors (i.e., against a laser tracker as the reference instrument) in this section.

We first consider the two cases where we do not fit the TLS error model, i.e, Case I and Case II. For Case I, the standard deviation of the angles is 2.3 arcseconds and 7.7 arcseconds while the standard deviation of the range is 0.49 mm. For Case II, the standard deviation of the angles increases substantially to 33.5 arcseconds and 44.4 arcseconds but the standard deviation of the range decreases to 0.04 mm.

An uncompensated TLS has large mechanical/optical misalignments, and these reflect as angular errors that change in sign between the faces. When considering only the data in the front-face of the TLS (Case I), the misalignment induced errors are not effectively captured, resulting in an apparent agreement between the different TLS positions. This leads to smaller angular standard deviations. However, the attempt to minimize the angular residuals through the least-squares process inflates the range residuals, hence the larger range standard deviation. It is worth noting again that the larger range standard deviation is an artifact of the least-squares process and does not represent actual TLS range variability

Table 1
TLS A intrinsic errors in terms of standard deviation along ranging and angular directions.

Case	Description	Horizontal angle (arcseconds)	Vertical angle (arcseconds)	Range (mm)	Inter-target distance uncertainty ($k = 2$)
I	Front-face only, no model fitting	2.3	7.7	0.49	0.22 mm to 0.74 mm
II	Front-face and back-face, no model fitting	33.5	44.4	0.04	0.05 mm to 0.96 mm
III	Front-face and back-face, with model fitting	3.0	7.6	0.04	0.07 mm to 0.23 mm

Note: With 20 targets and 4 TLS positions, there are 80 residuals each along the ranging, horizontal angle, and vertical angle directions. The standard deviations are calculated on those 80 residuals.

across the four positions. When considering data from multiple TLS positions in both faces (Case II), the angular errors are now effectively captured, leading to larger and more realistic standard deviations. The smaller range residuals, and therefore smaller standard deviation, is also more realistic, and captures the actual range variability present in the TLS.

The large range standard deviation for Case I and large angular standard deviations for Case II result in distance uncertainties for Case I and II that are similar in magnitude, see last column in Table 1. To assess whether these distance uncertainties are reasonable, we compare them against the measured errors. Fig. 14(a) shows the uncertainties for Case I plotted against measured errors for the 190 inter-target distances. The measured errors are smaller than the estimated uncertainties for only 82 out of the 190 distances (i.e., 43.2 %) indicating that uncertainty estimates are not reasonable. Fig. 14(b) shows the uncertainties for Case II plotted against measured errors for the 190 inter-target distances. The uncertainty estimates improve, but the measured errors are smaller than the estimated uncertainties for only 96 of the 190 distances (50.5 %). These values and percentages are summarized in Table 2.

We now consider the case where we do fit the TLS error model, i.e., Case III. The standard deviation along the angles is 3.0 arcseconds and 7.6 arcseconds, while the standard deviation of the range is 0.04 mm, see Table 1. The angular standard deviations are smaller than those for Case II, even though data from both faces are used, because the error model accounts for mechanical and optical misalignments. As a result,

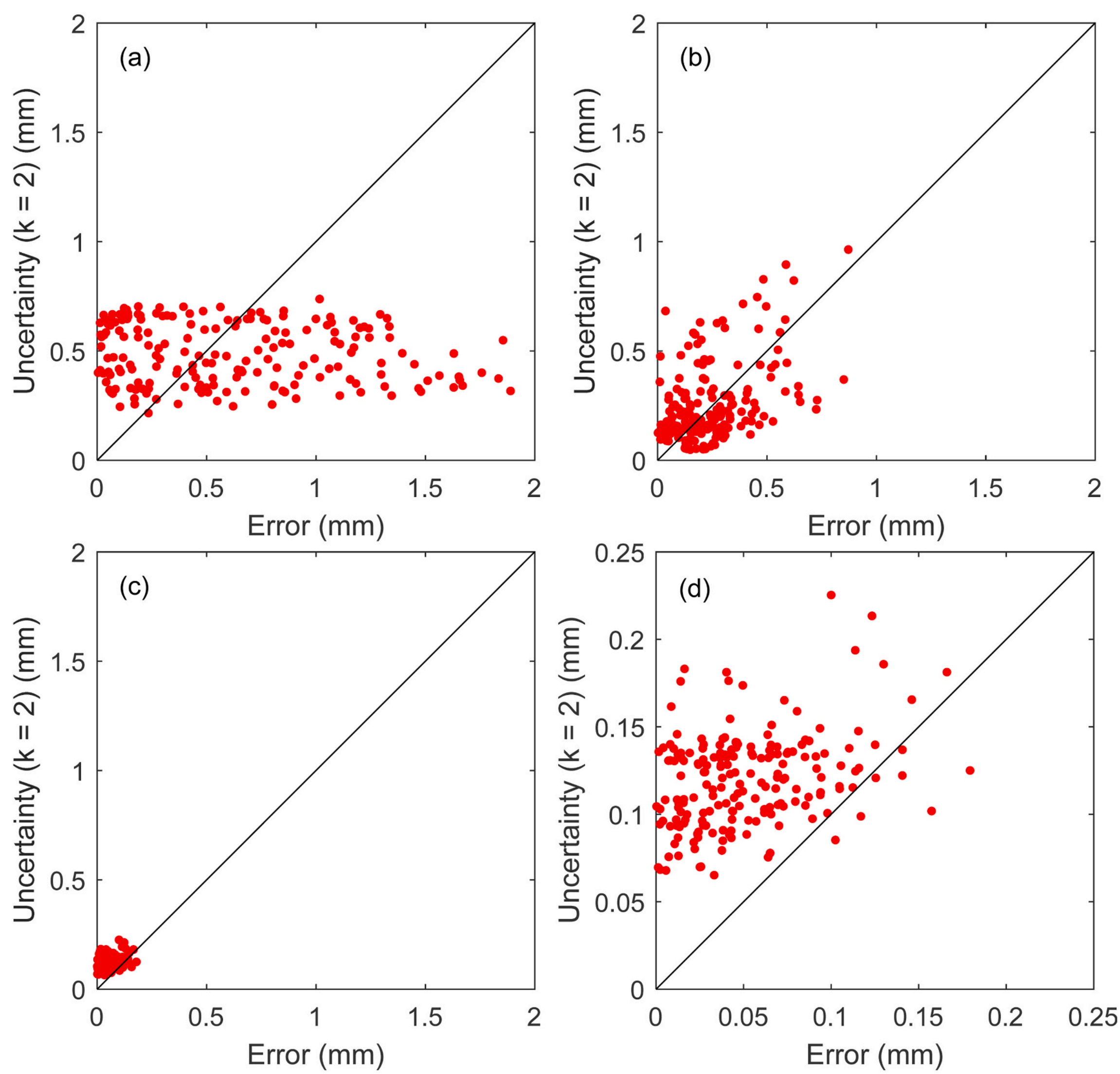

Fig. 14. Uncertainty vs error plot for TLS A: (a) Case I, front-face data only, no TLS error model (b) Case II, considering both front and back-face data, no TLS error model, (c) Case III, considering front-face and back-face data and fitting TLS error model, (d) same plot as in part (c) but rescaled to more clearly show the points.

Table 2
Number of inter-target distances whose measured errors are smaller than the estimated uncertainty ($k = 2$).

Case	# (out of a total of 190)	%
I	82	43.2
II	96	50.5
III	183	96.3

the data from the four TLS positions show better agreement (i.e., the data overlaps more closely). Fig. 14 (c) and (d) show the uncertainties for Case III plotted against the measured errors for the 190 inter-target distances. The uncertainty estimates are smaller than those for Case I and II. Moreover, the measured errors are smaller than the estimated uncertainties for 183 out of the 190 distances (96.3 %), indicating the validity of our method. Some error sources not captured by the model described in Appendix A, such as angle of incidence effects [33], may explain why the measured errors do not fall below the uncertainty estimates for all 190 distances.

For clarity, we note the following. Fig. 14 (a), (b), and (c) correspond to the uncertainty versus error plots for the errors in Fig. 11 (a), (b), and (c), respectively. Also, the values reported in Table 1, last column, represent the range of the uncertainty values shown in the Y-axis in Fig. 14 (a), (b), and (c).

A similar analysis is presented for TLS B below. Table 3 shows the standard deviations of the angles and the range calculated for the three cases. The uncertainty in each of the 190 inter-target distances are estimated by propagating these standard deviations. Fig. 15 (a), (b), and (c) show the uncertainty versus error plots corresponding to the errors in Fig. 13 (a), (b), and (c), respectively. The uncertainty estimates for Case I and Case II are not realistic, as the observed errors are larger than the estimated uncertainties, as seen in Fig. 15(a) and (b). Fig. 15 (c) and (d) show the uncertainties for Case III plotted against the measured errors for the 190 inter-target distances. The measured errors are smaller than the estimated uncertainties for 179 out of the 190 distances (94.2 %), indicating the validity of our method. As mentioned earlier, some error sources are not accounted for by the model described in Appendix A, such as angle of incidence effects [33], which might explain why the uncertainty estimates are not larger than the errors for all 190 distances. The number (and percentages) of distances whose measured errors are smaller than the estimated uncertainty is summarized in Table 4.

Before we proceed, we note an interesting difference between TLS A and TLS B. For TLS A, Case III (Fig. 14(c)) resulted in a reduction in both the errors and the uncertainty when compared to Case I. However, for TLS B, Case III (Fig. 15(c)) resulted in a reduction in errors only, not the uncertainty. TLS A had substantial systematic angular errors (as seen in Fig. 9(b)). Fitting the error model produced better estimates of the composite coordinates resulting in smaller errors. Fitting the error model also resulted in better agreement between the data from the different TLS positions resulting in smaller standard deviations and therefore, smaller uncertainties. TLS B did not have large systematic angular errors (as seen in Fig. 9(d)). Fitting the model captured some of the ranging errors resulting in better estimates of the composite coordinates resulting in smaller errors. Fitting the error model however did not result in substantial improvement in agreement between the data from the different TLS positions. Therefore, no significant change in standard deviations occurred, and therefore, no change in uncertainties.

For a poorly compensated TLS (with systematic angular errors), we have seen (from Fig. 14) that fitting the model improves agreement in the data between the different TLS positions, resulting in lower standard deviation of the residuals and therefore smaller uncertainties. Better agreement in the data between the positions does not automatically mean that the composite coordinates are closer to the true coordinates. Because the model that we employ has been extensively validated, the composite coordinates obtained through model fitting do result in smaller errors. For an already well compensated TLS (with random angular errors only), model fitting will not result in improved agreement in the data between the different TLS positions, thus uncertainties for all three cases will be the same. Because there are no underlying systematic errors in the TLS, all cases are expected to result in similar errors as well. That is, there is no advantage to model fitting over simple averaging for a well compensated TLS, i.e., one with negligible systematic angular errors.

Table 3
TLS B intrinsic errors in terms of standard deviation along ranging and angular directions.

Case	Description	Horizontal angle (arcseconds)	Vertical angle (arcseconds)	Range (mm)	Inter-target distance uncertainty ($k = 2$)
I	Front-face only, no model fitting	10.3	2.5	0.18	0.09 mm to 0.39 mm
II	Front-face and back-face, no model fitting	13.5	4.6	0.17	0.10 mm to 0.33 mm
III	Front-face and back-face, with model fitting	3.7	2.3	0.18	0.10 mm to 0.35 mm

Note: With 20 targets and 4 TLS positions, there are 80 residuals each along the ranging, horizontal angle, and vertical angle directions. The standard deviations are calculated on those 80 residuals.

5. Demonstration experiment

This experiment demonstrates the more typical application of our technique where planar targets are fixed at different positions in a room and measured from multiple positions of a TLS. Because a laser tracker cannot be used to establish the reference coordinates, we simply compared the results from the two TLSs that we used for this study.

5.1. Experimental setup

The demonstration experiment was conducted in a 13 m × 6.5 m × 3 m indoor space containing 20 contrast targets mounted on three walls. Laser tracker measurements were not possible in this case. The two TLSs were used to scan all 20 targets in both faces from four different positions. The data were processed following the procedure described in Sections 3.2.1, 3.2.2, and 3.2.3. Fig. 16 shows the layout of the target distribution and the TLS positions within the room.

5.2. Results

The composite coordinates of the 20 targets were computed for both TLSs and for all three cases. The 190 inter-target distances were then computed from these composite coordinates. For each of the TLSs, the intrinsic errors for the three cases are listed in Tables 5 and 6. These values were propagated to estimate the uncertainties in the inter-target distances. The range of values of these distance uncertainties for the 190 distances are also reported in Tables 5 and 6

To determine whether the inter-target distances calculated from the two TLSs agree with their respective uncertainties, i.e., their degree of equivalence [36,37], we performed the following calculation. Let d_A be the distance between a given pair of targets as measured by TLS A with an associated standard uncertainty u_A. Similarly, let d_B be the distance between the same pair of targets as measured by TLS B, with an associated standard uncertainty u_B. We then compute the absolute difference between the two distances and the uncertainty in that difference as follows:

$$\Delta = |d_A - d_B| \quad (14)$$

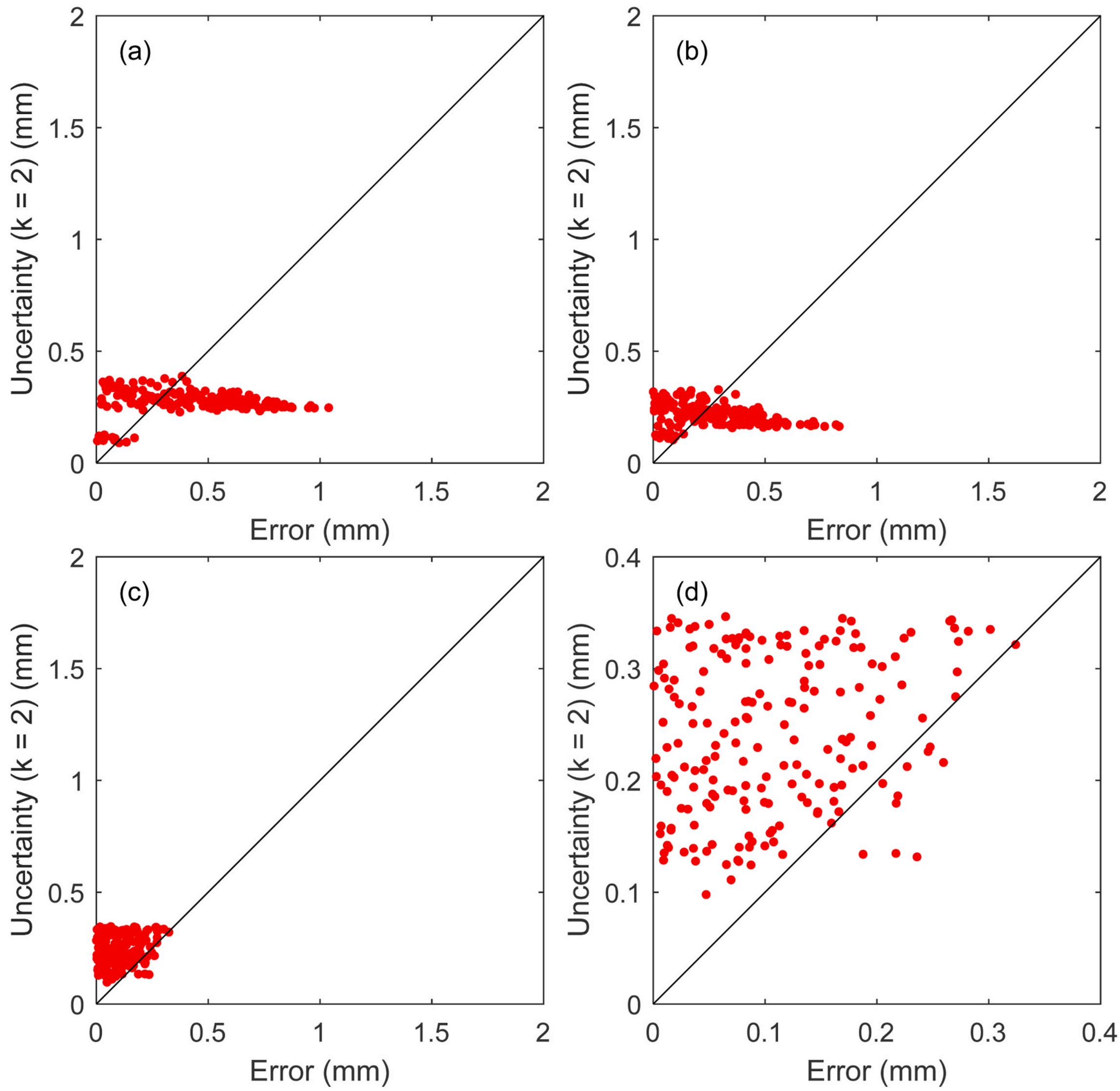

Fig. 15. Uncertainty vs error plot for TLS B: (a) Case I, front-face data only, no TLS error model (b) Case II, considering both front and back-face data, no TLS error model, (c) Case III, considering front-face and back-face data and fitting TLS error model, (d) same plot as in part (c) but rescaled to more clearly show the points.

Table 4
Number of inter-target distances whose measured errors are smaller than the estimated uncertainty ($k = 2$).

Case	# (out of a total of 190)	%
I	64	33.7
II	91	47.9
III	179	94.2

$$u_\Delta = \sqrt{(u_A^2 + u_B^2)} \quad (15)$$

Let the $k = 2$ expanded uncertainty in the difference, Δ, be $U_\Delta = 2u_\Delta$. If $\Delta < 2U_\Delta$, we conclude that the inter-target distance measured by the two TLSs agree within their uncertainties.

This computation was performed for all 190 inter-target distances for each case. The results are summarized in Table 7. For case I, only 45 out of the 190 distances (23.7 %) agree within their uncertainties. For case II, 128 out of the 190 distances (67.4%) agree within their uncertainties. Using only the front-face data (Case I) or using both front-face and back-face data without fitting the TLS error model (Case II) results in large distance errors, leading to poor agreement between the two TLSs. For case III, 189 out of the 190 distances (99.5 %) agree within their uncertainties. This exceptional agreement demonstrates the effectiveness of the proposed technique when the TLS error model is fit. For Case III, the calculated ($k = 2$) uncertainty for the inter-target distances ranged from approximately 0.06 mm to 0.23 mm for TLS A and from 0.09 mm to 0.39 mm for TLS B. These uncertainties are slightly larger than those of the validation experiment likely because the measurement volume is larger.

6. Discussion and conclusions

We have described the application of self-calibration to estimate inter-target distances with low uncertainty in a stationary network of targets using a terrestrial laser scanner (TLS). The technique was demonstrated using two TLSs, a short-range, high accuracy TLS with its internal error model turned off, and a long-range, lower accuracy TLS, within a measurement volume of 11 m × 6 m × 3 m. We obtained inter-target distance uncertainties below 0.2 mm ($k = 2$) for the short-range TLS even when it was fully uncompensated (i.e., internal error model turned off) and below 0.35 mm ($k = 2$) for the long-range TLS. The validity of these uncertainties was confirmed by comparing the measured distances against those obtained with a laser tracker. For more

Fig. 16. (a) Targets 1-16 and TLS positions 1, 2, and 4, (b) targets 10-20 and TLS positions 2-4.

Table 5
TLS A intrinsic errors in terms of standard deviation along ranging and angular directions, and inter-target distance uncertainty.

Case	Horizontal angle (arcseconds)	Vertical angle (arcseconds)	Range (mm)	Inter-target distance uncertainty ($k = 2$)
I	2.7	2.9	0.34	0.11 mm to 0.47 mm
II	33.5	44.2	0.06	0.06 mm to 0.73 mm
III	1.9	2.8	0.05	0.06 mm to 0.23 mm

Table 6
TLS B intrinsic errors in terms of standard deviation along ranging and angular directions, and inter-target distance uncertainty.

Case	Horizontal angle (arcseconds)	Vertical angle (arcseconds)	Range (mm)	Inter-target distance uncertainty ($k = 2$)
I	4.3	2.2	0.15	0.07 mm to 0.22 mm
II	11.2	4.1	0.14	0.09 mm to 0.38 mm
III	2.4	1.7	0.10	0.09 mm to 0.39 mm

than 94 % of the inter-target distances, the measured errors were smaller than the corresponding uncertainty estimates. In many cases, the inter-target distance errors obtained with our technique were an order of magnitude smaller than those from a single TLS position.

Table 7
Number of inter-target distances for which the distances calculated from the two TLSs agree with each other to within their uncertainties ($k = 2$).

Case	# (out of a total of 190)	%
I	45	23.7
II	128	67.4
III	189	99.5

There are two key requirements for implementing this technique:

First, the TLS must be able to scan each target in both the front-face and back-face orientations. Although most TLSs can measure in both faces, not all software packages allow users to export the scan data for each face separately. This limitation can be addressed by manufacturers providing software updates that provide users direct access to front- and back-face data. For our long-range TLS, we were able to obtain such access by collaborating directly with the manufacturer. The software for TLS A did allow the user to export scan data for each face separately.

Second, the ranging unit of the TLS must operate without significant linear (slope) or higher-order range errors, as these are not captured in the error model. This requirement is more challenging. Using a laser tracker, we determined that TLS B exhibited ranging errors on the order of 0.1 mm/m, which we were then able to correct. Without access to such high-end equipment, users must rely on periodic manufacturer calibration of their TLSs. However, this is a reasonable assumption given that the ranging unit contains no moving components and is generally stable over time.

Although not mentioned as a key requirement, temperature stability over the period of testing is also important. The experiments we reported on in this paper were performed in a laboratory that was temperature controlled to $20 \pm 0.5\,^{\circ}$C. Realizing uncertainties of 0.2 mm ($k = 2$) over 11 m in such a space is not an issue in such environment over a short period of time. When this technique is applied in a more industrial setting, temperature gradients and drift become an issue. Low-cost temperature loggers are available that can be used to record temperature over the scanning period to assess if the predicted uncertainties can in fact be met. Decreasing the scan resolution might also help speed up the data acquisition process, although lower resolution might result in larger composite center coordinate uncertainty.

Although our technique was motivated by the needs of the forensic community for an interim performance test, its applicability is much broader. It is well suited for geodesy, surveying, and manufacturing and assembly domains, where periodic performance assessments of dimensional metrology equipment are common. The method can be used to establish a calibrated network of targets that subsequently serves as a reference for the same TLS or for other lower-accuracy instruments.

CRediT authorship contribution statement

Bala Muralikrishnan: Writing – review & editing, Writing – original draft, Visualization, Validation, Software, Methodology, Investigation, Formal analysis, Data curation, Conceptualization. **Meghan Shilling:** Writing – review & editing, Validation, Software, Methodology, Formal analysis, Conceptualization. **Vincent Lee:** Writing – review & editing, Validation, Methodology, Investigation, Data curation. **Mary Gregg:** Writing – review & editing, Visualization, Validation, Software, Methodology, Investigation, Formal analysis, Data curation. **Dennis Everett:** Writing – review & editing, Validation, Methodology, Investigation, Data curation.

Disclaimer

Commercial equipment and materials may be identified in order to adequately specify certain procedures. In no case does such identification imply recommendation or endorsement by the National Institute of Standards and Technology, nor does it imply that the materials or equipment identified are necessarily the best available for the purpose.

Declaration of competing interest

The authors declare that they have no known competing financial interests or personal relationships that could have appeared to influence the work reported in this paper.

Acknowledgements

We thank Erica Romsos, JP Jones, and Henry Swofford at the Special Programs Office (SPO) at NIST for their support. We are grateful for funding from the Forensic Science Quality Assurance Program (FSQAP) and the Accelerating Forensic Innovation for Impact (AFI2) program sponsored by the SPO. We also thank the members of the CSIR subcommittee within OSAC for their feedback. Finally, we thank Octavio Icasio Hernandez (CENAM/NIST) and Shaw Feng (NIST) for their review of this document.

Appendix A

We present the TLS error model here for purposes of completeness. The TLSs under study (schematic shown in Fig. A1) consisted of a base, laser source, spinning platform, horizontal angle encoder, vertical angle encoder, and a spinning prism mirror. The measured range (r_m), horizontal angle (θ_m), and vertical ($\varnothing_m$) suffer from errors due to different geometric/optical misalignments in the system. In this paper we use the revised geometric error model reported by Wang et al. [29] to determine the corrections to the measured coordinates. We specify the error model below for purposes of completeness:

$$\Delta r_m = k(x_2 \sin \varnothing_m) + x_{10} \tag{A1}$$

$$\Delta\theta_m = k\left[\frac{x_{1z}}{r_m \tan \varnothing_m} + \frac{x_3}{r_m \sin \varnothing_m} + \frac{x_{5z7}}{\tan \varnothing_m} + \frac{2x_6}{\sin \varnothing_m} - x_{8x} \sin \theta_m + x_{8y} \cos \theta_m\right] + \frac{x_{1n}}{r_m} + x_{5n} + x_{11a} \cos 2\theta_m + x_{11b} \sin 2\theta_m \tag{A2}$$

$$\Delta\varnothing_m = k\left[\frac{x_{1n} \cos \varnothing_m}{r_m} + \frac{x_2 \cos \varnothing_m}{r_m} + x_4 + x_{5n9n} \cos \varnothing_m\right] - \frac{x_{1z} \sin \varnothing_m}{r_m} - x_{5z9z} \sin \varnothing_m + x_{12a} \cos 2\varnothing_m + x_{12b} \sin 2\varnothing_m \tag{A3}$$

where:

k is 1 for the front-face measurement and -1 for the back-face measurement.
r_m, θ_m, and $\varnothing_m$ are the measured range, horizontal angle and vertical angle, respectively.
$\Delta r_m, \Delta\theta_m, and\ \Delta\varnothing_m$ are corrections to the measured range, horizontal angle, and vertical angle.
x_{1n} and x_{1z} are beam offset along the N and Z axes, respectively.
x_2 is the transit offset.
x_3 is the mirror offset.
x_4 is the vertical index offset.
x_{5n} is the beam tilt along the N axis.
$x_{5z7} = x_{5z} - x_7$. x_{5z} is the beam tilt along the Z axis. x_7 is the transit tilt.
$x_{5n9n} = x_{5n} + x_{9n}$. x_{9n} is the vertical angle encoder eccentricity along the N axis.
$x_{5z9z} = x_{5z} + x_{9z}$. x_{9z} is the vertical angle encoder eccentricity along the Z axis.
x_6 is the mirror tilt.
x_{8x} and x_{8y} are horizontal angle encoder eccentricity along the X and Y axes, respectively.
x_{10} is the zero offset.
x_{11a} and x_{11b} are second order scale errors in the horizontal angle encoder.
x_{12a} and x_{12b} are second order scale errors in the vertical angle encoder.

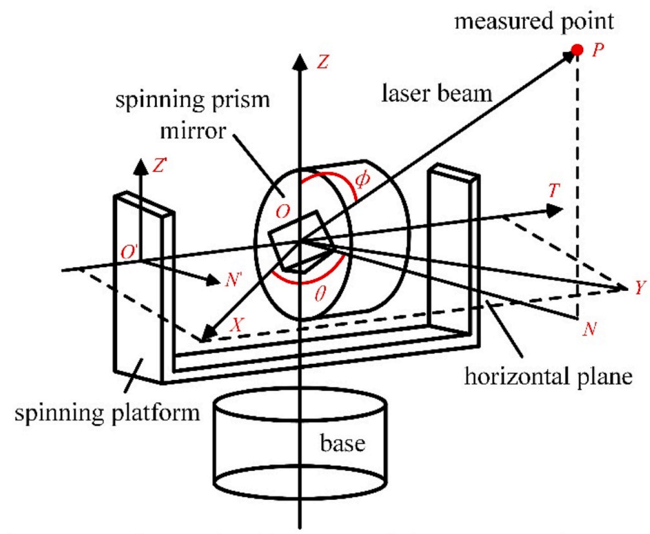

Fig. A1. Schematic diagram of the TLS under study

References

[1] Staiger R. 10 years of terrestrial laser scanning—technology, systems and applications, GEO-Siberia. 26–29 April, 2011. Novosibirsk, Russia.
[2] Shan J, Toth CK, editors. Topographic laser ranging and scanning: principles and processing. Boca Raton, FL: CRC Press; 2009.
[3] ASTM E3125–17. Standard test method for evaluating the point-to-point distance measurement performance of spherical coordinate 3D imaging systems in the medium range. 2017.
[4] ASTM E2938-15. Standard test method for evaluating the relative-range measurement performance of 3D imaging systems in the medium range. 2015.
[5] ISO 17123-9: 2018. Optics and optical instruments — Field procedures for testing geodetic and surveying instruments. Part 9: Terrestrial laser scanners.
[6] Muralikrishnan B. Performance evaluation of terrestrial laser scanners – a review. Meas Sci Technol 2021;32(7). https://doi.org/10.1088/1361-6501/abdae3.
[7] Gregg M, Muralikrishnan B, Shilling M. Toward a documentary standard for performance testing of terrestrial laser scanners used in forensic practice: a statistical procedure to assess change in instrument precision. J. Forensic Sci. 2026; 71:1023–31. https://doi.org/10.1111/1556-4029.70256.
[8] Muralikrishnan B, Shilling M, Gregg M, Lee V, Keller J, Casey E, Liscio E, O'Neil B, Russ M, Terpstra T. Report on the May 2025 NIST measurement week: realization of an OSAC draft interim performance assessment for terrestrial laser scanners used by law enforcement agencies. National Institute of Standards and Technology Internal Report; 2025. NISTIR 8583. doi: 0.6028/NIST.IR.8583.
[9] OSAC website, https://www.nist.gov/adlp/spo/organization-scientific-area-committees-forensic-science, accessed on June/18/2025.
[10] International vocabulary of metrology—basic and general concepts and associated terms (VIM). Joint committee for guides in metrology, JCGM 200:2012. (third ed.). doi:10.59161/JCGM200-2012.
[11] Rietdorf A, Gielsdorf F, Gruendig L. Combination of hand measuring methods and scanning techniques. April 2003. p. 13–7. Paris, France.
[12] Gielsdorf F, Rietdorf A, Gruendig L. A concept for the calibration of terrestrial laser scanners. Proceedings FIG Working Week. May 2004. p. 22–7. Athens, Greece.
[13] Lichti DD, Franke J. Self-calibration of the iQsun 880 laser scanner. In: Proceedings of the Optical 3-D Measurement Techniques VII. Vienna, Austria; 2005. p. 122–31.
[14] Lichti DD, Licht MG. Experiences with terrestrial laser scanner modelling and accuracy assessment. Int. Arch. Photogramm. Remote Ses. Spatial Inf. Sci. 2006;36 (Part 5):155–60.
[15] Lichti DD. Error modelling, calibration and analysis of an AM-CW terrestrial laser scanner system. ISPRS J. Photogramm. Remote Sens. 2007;61:307–24. https://doi.org/10.1016/j.isprsjprs.2006.10.004.
[16] Reshetyuk Y. Calibration of terrestrial laser scanners for the purposes of geodetic engineering. In: 3rd IAG symposium on Geodesy for Geotechnical and Structural Engineering and 12th FIG Symposium on Deformation Measurements. Austria: Baden; 2006.
[17] Abbas MA, Lichti DD, Chong AK, Setan H, Majid Z. An on-site approach for the self-calibration of terrestrial laser scanner. Measurement 2014;52:111–23. https://doi.org/10.1016/j.measurement.2014.03.009.
[18] González-Aguilera D, Rodríguez-Gonzálvez P, Armesto J, Arias P. Trimble GX200 and Riegl LMS-Z390i sensor self-calibration. Opt. Express 2011;19(3):2676–93. https://doi.org/10.1364/OE.19.002676.
[19] Holst C, Kuhlmann H. Aiming at self-calibration of terrestrial laser scanners using only one single object and one single scan. J. Appl. Geodesy 2014;8(4):295–310. https://doi.org/10.1515/jag-2014-0017.
[20] Schneider DR. Calibration of a Riegl LMS-Z420i based on a multi-station adjustment and a geometric model with additional parameters. Int. Arch. Photogramm. Remote Ses. Spatial Inf. Sci. 2009;38:177–82.
[21] Chan TO, Lichti DD, Belton D. A rigorous cylinder-based self-calibration approach for terrestrial laser scanners. ISPRS J. Photogramm. Remote Sens. 2015;99:84–99. https://doi.org/10.1016/j.isprsjprs.2014.11.003.
[22] García-San-Miguel D, Lerma JL. Geometric calibration of a terrestrial laser scanner with local additional parameters: an automatic strategy. ISPRS J. Photogramm. Remote Sens. 2013;79:122–36. https://doi.org/10.1016/j.isprsjprs.2013.02.007.
[23] Al-Manasir K., Lichti D. Self-calibration of a Lecia HDS7000 scanner. FIG Working Week; 2015. Sofia, Bulgaria.
[24] Bae K-H, Lichti DD. On-site self-calibration using planar features for terrestrial laser scanners. Int. Arch. Photogramm. Remote Ses. Spatial Inf. Sci. 2007;36:14–9.
[25] Chow JCK, Lichti DD, Glennie C, Hartzell P. Improvements to and comparison of static terrestrial LiDAR self-calibration methods. Sensors 2013;13:7224–49. https://doi.org/10.3390/s130607224.
[26] Abmayr T, Dalton G, Härtl F, Hines D, Liu R, Hirzinger G, Fröhlich C. Standardization and visualization of 2.5D scanning data and color information by inverse mapping. Optical 3D Measurement Techniques VII: Applications in GIS, Mapping, Manufacturing, Quality Control, Robotics, Navigation, Mobile Mapping, Medical Imaging, VR Generation, and Animation. 2005. October 3-5.
[27] Neitzel F. Investigation of axes errors of terrestrial laser scanners. Proceedings of the Fifth Int. Symp. Turkish-German Joint Geodetic Days. 2006. Berlin, Germany, March 29-31.
[28] Neitzel F. Untersuchung des ackssytems und des taumelfehlers terrestrischer laserscanner mit tachymetrischem messprinzip. Terrestrisches Laser-Scanning (TLS 2006) Schriftenreihe Des DVW 51 15–34 Augsburg: wißner-verlag. 2006.
[29] Wang L, Muralikrishnan B, Rachakonda P, Sawyer D. Determining geometric error model parameters of a terrestrial laser scanner through two-face, length-consistency, and network methods. Meas. Sci. Technol. 2017;28. https://doi.org/10.1088/1361-6501/aa6929.
[30] Muralikrishnan B, Ferrucci M, Sawyer D, Gerner G, Lee V, Blackburn C, Phillips S, Petrov P, Yakovlev Y, Astrelin A, Milligan S, Palmateer J. Volumetric performance evaluation of a laser scanner based on geometric error model. Precis. Eng. 2015;40: 139–50. https://doi.org/10.1016/j.precisioneng.2014.11.002.
[31] Shi S, Muralikrishnan B, Sawyer D. Terrestrial laser scanner calibration and performance evaluation using the network method. Opt. Lasers Eng. 2020;134: 106298. https://doi.org/10.1016/j.optlaseng.2020.106298.
[32] Icasio-Hernández O, Aldo Bellelli D, Brum Vieira LH, Cano D, Muralikrishnan B. Validation of the network method for evaluating uncertainty and improvement of geometry error parameters of a laser tracker. Precis. Eng. 2021;72:664–79. https://doi.org/10.1016/j.precisioneng.2021.07.005.
[33] Muralikrishnan B, Lu X, Gregg M, Shilling M, Czapla B. A method to evaluate orientation-dependent errors in the center of contrast targets used with terrestrial laser scanners. Sensors 2025;25(2):505. https://doi.org/10.3390/s25020505.
[34] Rachakonda P, Muralikrishnan B, Sawyer D. Metrological evaluation of contrast target center algorithm for terrestrial laser scanners. Measurement 2019;134: 15–24. https://doi.org/10.1016/j.measurement.2018.08.039.

[35] Calkins JM. Quantifying coordinate uncertainty fields in coupled spatial measurement systems. PhD dissertation. Virginia Polytechnic Institute and State University; 2002.
[36] Taylor JR. Error analysis. Sausalito, California: Univ. Science Books; 1997.
[37] Cox MG. The evaluation of key comparison data. Metrologia 2002;39(6). https://doi.org/10.1088/0026-1394/39/6/10.